ORIGINAL PAPER

A coupled numerical–experimental study of the breakage process of brittle substances

Hadi Haeri · Kourosh Shahriar ·
Mohammad Fatehi Marji · Parviz Moarefvand

Abstract Pre-existing cracks in brittle substances seem to be the main cause of their breakage under various loading conditions. In the present paper, a coupled numerical–experimental analysis of crack propagation, cracks coalescence, and breakage process of brittle substances such as rocks and rock-like samples have been studied. The numerical analyses are accomplished using a numerical code based on the Higher order Displacement Discontinuity Method for Crack (HDDMCR^{2D}) analysis. A quadratic displacement discontinuity variation along each boundary element is assumed to evaluate the Mode I and Mode II stress intensity factors. Based on the linear elastic fracture mechanics theory, the maximum tangential stress criterion (i.e., a mixed mode fracture criterion) is implemented in the HDDMCR^{2D} code for predicting the crack initiation and its direction of propagation (cracks propagation path). Some numerical and analytical problems in finite and infinite planes are solved numerically by the proposed numerical method, and the results are compared in different tables illustrating the accuracy and validity of the numerical results. Experimental tests are also being done to evaluate the final breakage path and cracks initiation and cracks coalescence stresses in rock-like specimens containing two random cracks. The numerical and experimental results obtained from the tested specimens show a good agreement between the corresponding values and demonstrate the accuracy and effectiveness of the approach.

Keywords Cracks · Breakage path · Rock-like specimen · HDDMCR^{2D} · Numerical and experimental analyses

H. Haeri (✉)
Department of Mining Engineering, Science and Research Branch,
Islamic Azad University, Tehran, Iran
e-mail: hadihaeri@ymail.com

K. Shahriar
Department of Mining and Metallurgical Engineering,
Amirkabir University of Technology, Tehran, Iran

M. F. Marji
Faculty of Mining and Metallurgy, Institution of Engineering,
Yazd University, Yazd, Iran

P. Moarefvand
Department of Mining and Metallurgical Engineering,
Amirkabir University of Technology, Tehran, Iran

Introduction

The mechanical properties and breakage mechanisms of the pre-existing fractures and discontinuities may play a vital role to understand the physico-mechanical characteristics of a rock mass surrounding rock structures such as surface and underground mines, tunnels, rock slopes, etc. (Ke et al. 2008; Verma and Singh 2010; Ma et al. 2012; Al Fouzan and Dafalla 2013).

One of the most effective issues on the mechanical behaviors of brittle materials (such as rocks) is the presence of pre-existing cracks (Golshani et al. 2005). Although the mechanical behavior of rocks may depend on their mechanical structure, the extension of pre-existing cracks depends on the properties such as size, position, orientation, and loading condition. The cracks typically nucleate at the places of stress concentrations like pores, inclusions, sharp cracks, and triple connections (Haeri et al. 2013).

Ichikawa et al. (2001) indicated that the production and propagation of cracks play an important role in predicting the cyclic breakage process of rocks. The resulted cracks may be further extended in kinked or curved forms (Marji and Dehghani 2010). The breakage mechanism of brittle substances with randomly oriented cracks depends on the degree of interaction between cracks and their coalescence path (Li and Yang 2001). There are generally two mechanisms of quasi-static crack propagation and cracks coalescence, which may be observed in the experimental and numerical studies of

the brittle materials specimens under various loading conditions (Manouchehrian and Marji 2012; Afifipour and Moarefvand 2013).

The pre-existing cracks in rocks are normally under compressive loading rather than under tension, shear, or mixed mode loading (Ke et al. 2008). In compressive loading, one might therefore expect that crack initiation will follow in the direction (approximately) parallel to the major principal compressive stress (Hoek and Bieniawski 1965). In the breakage process of the brittle substances under uniaxial compression, two types of cracks may be observed originating from the original tips of pre-existing cracks (i.e., wing cracks and secondary cracks as shown in Fig. 1). Wing cracks may generally be considered as the emanating tensile cracks that initiate at or near the original tips of the pre-existing cracks in a specimen under loading. These tensile cracks may propagate in a curved path form and parallel to the direction of major principal compressive stress. The secondary cracks may be considered as shear cracks that may initiate from the original tips of the pre-existing cracks and propagate in a stable manner. These shear cracks may initiate in two different directions, i.e., coplanar (quasi-coplanar) and/or oblique to the direction of pre-existing cracks (Bobet and Einstein 1998a, b).
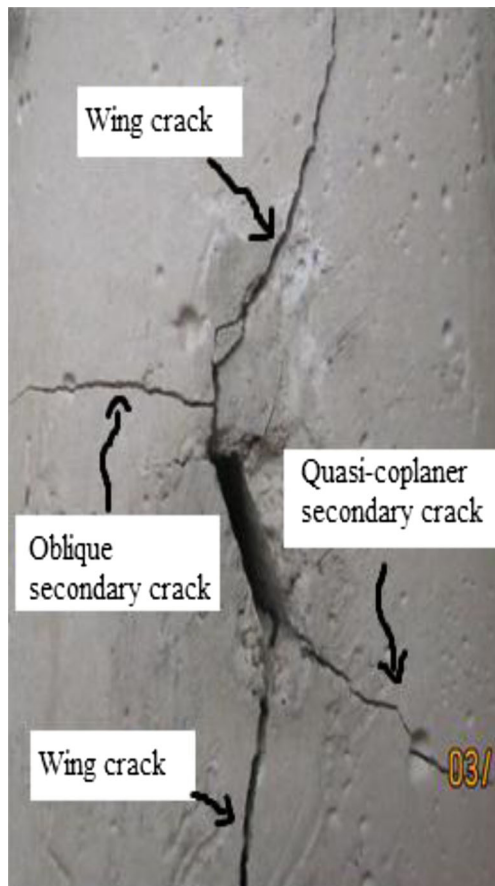

Fig. 1 A propagated center slant crack under uniaxial compression

Many experimental procedures have been reported on various types of rock or rock-like substances under compressive loading (Ingraffea 1985; Horii and Nemat-Nasser 1985; Huang et al. 1990; Reyes and Einstein 1991; Shen et al. 1995; Wong and Chau 1998; Wong et al. 2001; Sahouryeh et al. 2002; Sagong and Bobet 2002; Li et al. 2005; Wong and Einstein 2006; Park 2008; Park and Bobet 2009; Yang et al. 2009). Recently, Park and Bobet (2010) conducted experimental tests on rock-like samples, each containing three cracks and explored differences and similarities between open and closed cracks. According to their findings, different modes of initiation and propagation of cracks were recognized. Moreover, various types of cracks coalescence were observed for specimens containing open or closed cracks. In another research work, Janeiro and Einstein (2010) conducted uniaxial compression tests to investigate the cracking behavior of prismatic gypsum specimens containing one or two inclusions. In addition, Yang (2011) studied the effect of coplanar crack angle on the strength and deformation behavior in sandstone samples. The crack initiation and coalescence of samples containing two coplanar cracks were observed using photographic monitoring from the tips of pre-existing coplanar cracks. As a result of this research, a relationship between the coplanar crack angle and the crack coalescence stress was presented. Lee and Jeon (2011) applied uniaxial compression test on three different materials to experimentally analyze the crack initiation, propagation, and coalescence of pre-existing single and double cracks. In addition, the crack initiation and coalescence stresses were investigated in their study showing that the crack initiation and propagation depends on the type of material. Ghazvinian et al. (2012) experimentally studied the effect of crack inclination angle and crack length on fracturing processes of brittle materials under diametrical compression.

Despite the improvements made in the experimental observation of the various types of rock or rock-like substances under compression, several numerical or analytical–numerical approaches (due to their high accuracy, reliability, and lower costs) were also used for modeling the rock breakage mechanism (Haeri 2011). In this respect, various numerical methods have been developed for the simulation of crack propagation in brittle substances, e.g., finite element method (FEM) (Oliver et al. 2006; Li and Wong 2012), boundary element method (BEM) (Crouch and Starfield 1983), discrete element method (Manouchehrian and Marji 2012), discontinuous Galerkin method (Sukumar et al. 1997; Stan 2008), and mesh-free methods (Rabczuk et al. 2007; Bordas et al. 2008). Based on these numerical methods, several computer codes have also been developed for modeling the breakage mechanism of brittle materials such as rocks, e.g., FROCK code (Park 2008), Rock Failure Process Analysis (RFPA^{2D}) code (Wong et al. 2002), and 2D Particle Flow Code (PFC^{2D}) (Lee and Jeon 2011; Manouchehrian and Marji 2012; Ghazvinian et al. 2012).

Oguni et al. (2009) developed a new method, called particle discretization scheme finite element method (PDS–FEM), which can be used for the quasi-static analysis of crack propagation.

Three important breakage initiation criteria were proposed to study the crack propagation mechanism of brittle materials: (1) the maximum tangential stress criterion (σ-criterion) (Erdogan and Sih 1963), (2) the maximum energy release rate criterion (G-criterion) (Hussian et al. 1974), and (3) the minimum energy density criterion (S-criterion) (Sih 1974). Some modified form of the mentioned criteria, e.g., F-criterion, which is a modified energy release rate criterion proposed by Shen and Stephansson (1994), may also be used to study the breakage behavior of brittle substances (Marji et al. 2006; Marji 2013). Recently, Behnia et al. (2011) have compared the σ-criterion and S-criterion for crack propagation analysis in rocks (for a Poisson's ratio of 0.2) and obtained almost the same results for both criteria.

Methodology

In this study, a comprehensive analytical, numerical, and experimental approach is developed for the analyses of cracks initiation, propagation, and coalescence in rocks and rock-like substances. For this purpose, a modified indirect boundary element method based on displacement discontinuities along a straight-line crack is developed. Then a computer code (HDDMCR^{2D}) is prepared using a quadratic variation of displacement discontinuities with three equal sub-elements. This numerical approach may be regarded as a mesh reducing dual boundary element method (Chen and Hong 1999; Aliabadi 1998) for solving two-dimensional elastostatic problems where the cracks are discretized as straight lines (not as two separate overlapped lines as considered in the conventional direct dual boundary element method). It should be noted that the Mode I and Mode II strain energy release rate and the Mode I and Mode II stress intensity factors are interrelated for the brittle substances such as rocks. The G-

criterion and its modified form (F-criterion) have also been used in the literature. The differences between these criteria may be evident for the case of ductile substances such as steels. Recently, Behnia et al. (2011) have compared the σ-criterion and S-criterion for crack propagation analysis in layered rocks (for a Poisson's ratio of 0.2) and obtained almost the same results for both criteria. Therefore, the σ-criterion may be used for the crack propagation analysis of brittle rocks (as have been used by many researchers such as Whittaker et al. 1992; Haeri et al. 2013; Behnia et al. 2013).

Results of the numerical analysis are compared with the existing analytical results or with the performed experimental work results. The breakage mechanism of brittle substances due to the propagation and coalescence of random cracks have been studied. The linear elastic fracture mechanics (LEFM) concepts [by computing the Mode I and Mode II stress intensity factors (SIFs)] and σ-criterion have been implemented in the computer code to predict the possibility of crack propagation and estimate the crack initiation direction. An iterative method explained by Marji (1997) has been used to investigate the crack propagation direction and path after each crack extension, $\Delta b = 0.1b$, successively. To investigate the cracks coalescence phenomenon, two small random cracks are considered at the central part of a finite plate under uniaxial compression. The crack propagation path of each crack has been estimated by the iterative method and the coalescence of the cracks has been observed. Some experimental works are also accomplished by testing specially prepared rock-like samples [prepared by mixing Portland Pozzolana Cement (PPC), fine sand, and water] containing central single and double cracks. The specially prepared rock-like specimens were tested under compressive loading in a rock mechanics laboratory to visualize the cracks propagation and cracks coalescence processes. Comparing the numerical results with both the analytical and experimental results demonstrates the accuracy and effectiveness of the proposed numerical method in the study of the rock breakage process under compressive loading conditions.

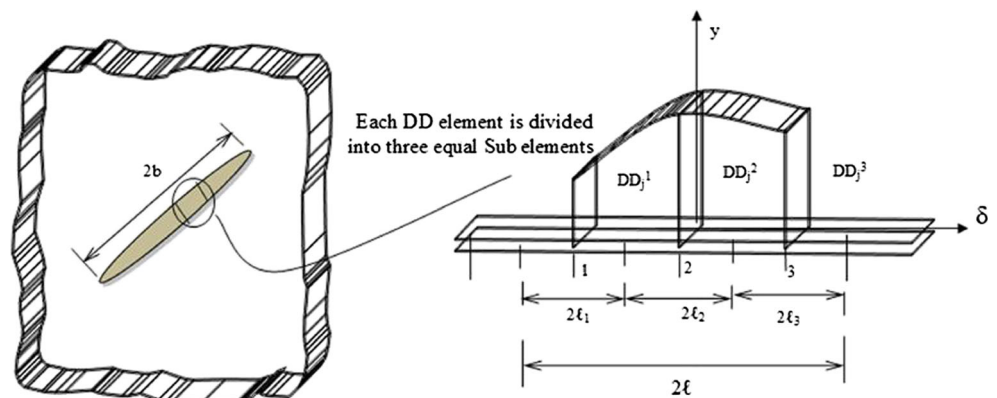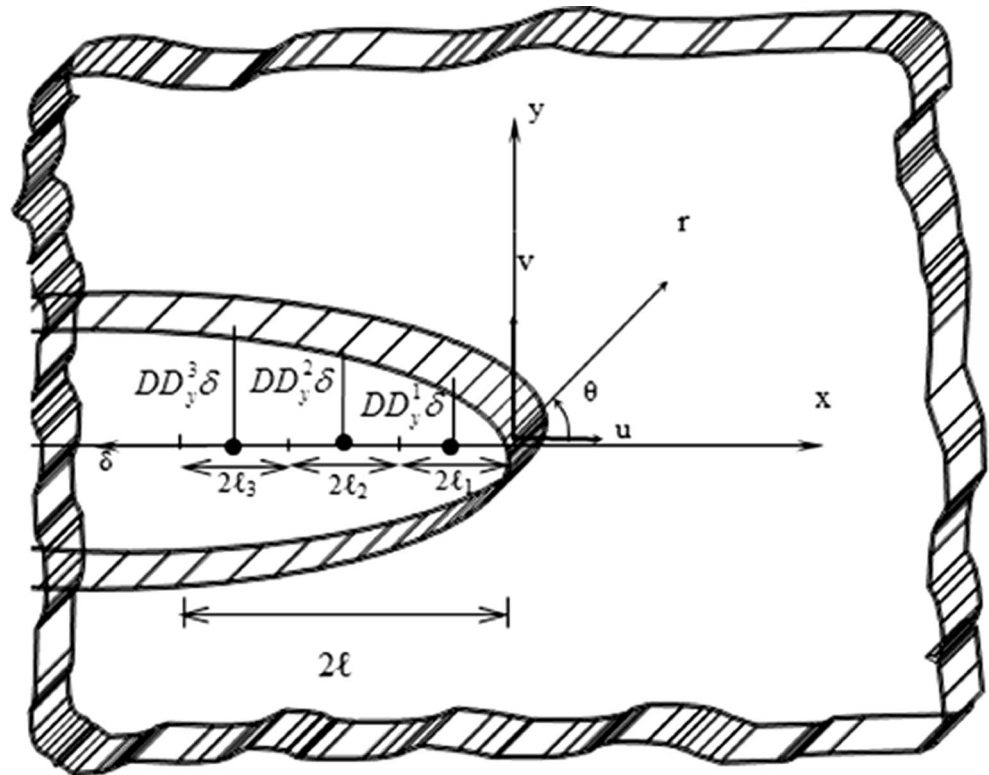Fig. 2 Discretization of a center slant crack into quadratic DD elements

Higher order displacement discontinuity method

Higher order displacement discontinuity method (HDDM) is a
category of the broad indirect BEM for solving the elastostatic
problems with specified boundary conditions by assuming
continuous stress and discontinuous displacement fields at
the discretized boundaries. In this method, the boundaries
are discretized into a proper number of line crack elements
(Guo et al. 1990, 1992; Scavia 1990; Aliabadi and Rooke
1991; Aliabadi 1998; Marji et al. 2006; Haeri and Ahranjani
2012; Marji 2013; Haeri et al. 2013).

In this research, in order to obtain a higher accuracy of the
displacement discontinuities (DDs) along the boundary of the
problem, a two-dimensional HDDM employing quadratic
elements is used. A quadratic DD element is divided into three
equal sub-elements that each sub-element contains a central
node for which the nodal DDs are evaluated numerically
(Marji et al. 2006).

Based on this definition of DD, it can be formulated as:

$$\mathrm{DD}_j(\delta) = \sum_{i=1}^{3} \Gamma_i(\delta)\mathrm{DD}_j^i , \; j = x, y \qquad (1)$$

where $\mathrm{DD}_j{}^1$, $\mathrm{DD}_j{}^2$, and $\mathrm{DD}_j{}^3$ are the quadratic nodal displace-
ment discontinuities in x and y directions. Considering a
quadratic element of length, 2ℓ , with equal sub-elements
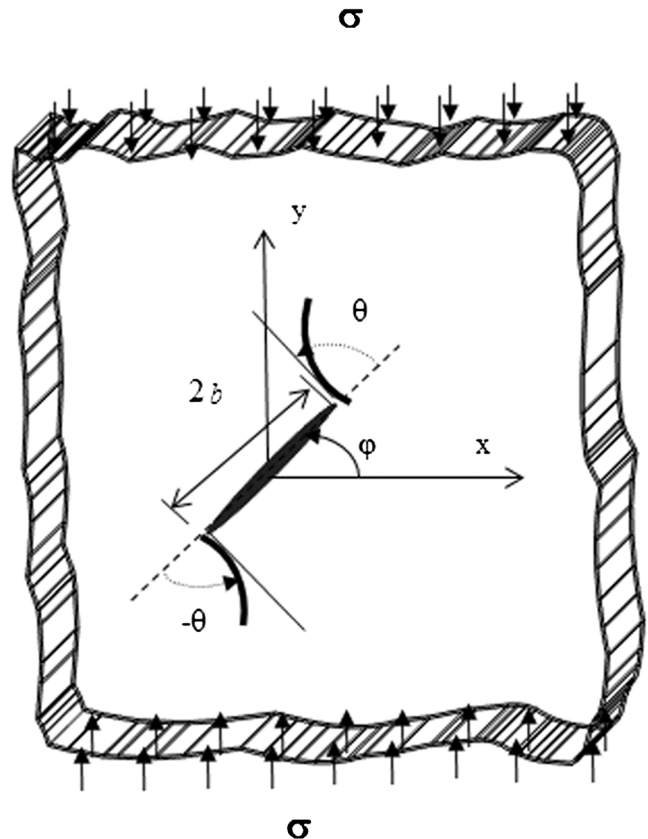$(\ell_1 = \ell_2 = \ell_3)$ and a quadratic shape function, $\Gamma_i(\delta)$ for −

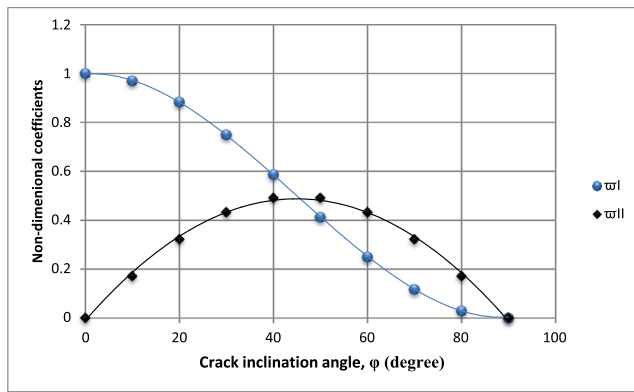Fig. 4 A center slant crack in an infinite plane

Fig. 5 Variation of ϖ_I and ϖ_{II} with crack inclination angles

$\ell \leq \delta \leq \ell$, the following shape functions can be defined (Marji et al. 2006).

$$\begin{aligned} \Gamma_1(\delta) &= -\left(3\ell_1^3 - \ell_1^2\delta - 3\ell_1\delta^2 + \delta^3\right)/\left(48\ell_1^3\right), \\ \Gamma_2(\delta) &= \left(9\ell_1^3 - 9\ell_1^2\delta - \ell_1\delta^2 + \delta^3\right)/\left(16\ell_1^3\right), \\ \Gamma_3(\delta) &= \left(9\ell_1^3 + 9\ell_1^2\delta - \ell_1\delta^2 - \delta^3\right)/\left(16\ell_1^3\right) \end{aligned} \quad (2)$$

A quadratic element has three nodes, which are at the centers of its three sub-elements as shown in Fig. 2. The derivation of shape functions for a quadratic variation of displacement discontinuity along the boundary element and their implementation in the modified HDDMCR²ᴰ code is explained in Appendix 1 for both infinite and finite plane problems.

Since the singularities of the stresses and displacements near the crack ends may reduce their accuracies, special crack tip elements are used to increase the accuracy of the DDs near the crack tips (Marji et al. 2006). As shown in Fig. 3, the DD variation for three nodes can be formulated using a special crack tip element containing three nodes (or having three special crack tip sub-elements)

$$\mathrm{DD}_j(\delta) = [\Gamma_{C1}(\delta)]\mathrm{DD}_j^1(\ell) + [\Gamma_{C2}(\delta)]\mathrm{DD}_j^2(\ell) + [\Gamma_{C3}(\delta)]\mathrm{DD}_j^3(\ell) \quad (3)$$

where the crack tip element has a length $\ell = \ell_1 + \ell_2 + \ell_3$. Considering a crack tip element with the three equal sub-

Table 1 Mechanical properties of the rock-like specimens (obtained experimentally in a rock mechanics laboratory)

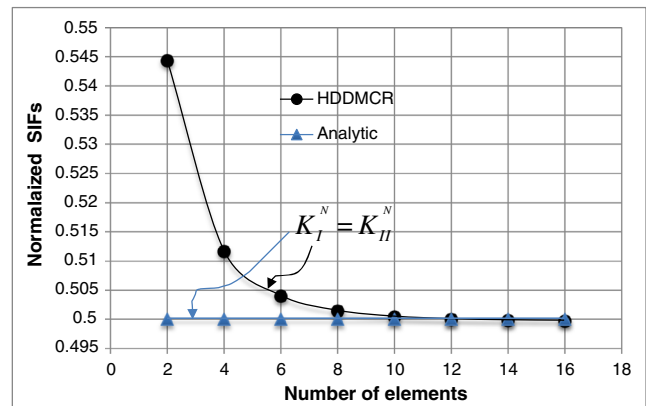| Description	Parameter	Value	Unit
Crack length	$2b$	10	mm
Uniaxial compression strength	σ	26	MPa
Modulus of elasticity	E	17	GPa
Poisson's ratio	ν	0.2	–
Fracture toughness	K_{IC}	2	MPa m$^{1/2}$

Fig. 6 The normalized SIFs $\left(K_I^N = K_{II}^N\right)$ for the 45° center crack ($\varphi = 45°$) using different number of elements and a constant $L/b = 0.2$

elements ($\ell_1 = \ell_2 = \ell_3$) , the shape functions $\Gamma_{C1}(\delta)$, $\Gamma_{C2}(\delta)$ and $\Gamma_{C3}(\delta)$ can be obtained as equations:

$$\begin{aligned} \Gamma_{C1}(\delta) &= \frac{15\delta^{\frac{1}{2}}}{8\ell_1^{\frac{1}{2}}} - \frac{\delta^{\frac{3}{2}}}{\ell_1^{\frac{3}{2}}} + \frac{\delta^{\frac{5}{2}}}{8\ell_1^{\frac{5}{2}}}, \\ \Gamma_{C2}(\delta) &= \frac{-5\delta^{\frac{1}{2}}}{8\ell_1^{\frac{1}{2}}} + \frac{3\delta^{\frac{3}{2}}}{2\sqrt{3}\ell_1^{\frac{3}{2}}} - \frac{\delta^{\frac{5}{2}}}{4\sqrt{3}\ell_1^{\frac{5}{2}}}, \\ \Gamma_{C3}(\delta) &= \frac{3\delta^{\frac{1}{2}}}{8\sqrt{5}\ell_1^{\frac{1}{2}}} - \frac{\delta^{\frac{3}{2}}}{2\sqrt{5}\ell_1^{\frac{3}{2}}} + \frac{\delta^{\frac{5}{2}}}{8\sqrt{5}\ell_1^{\frac{5}{2}}} \end{aligned} \quad (4)$$

The derivation of these shapes functions and their implementation in the modified HDDMCR²ᴰ code is explained in Appendix 2 for completeness.

Based on the LEFM principles, the Mode I and Mode II stress intensity factors K_I and K_{II} (MPa m$^{1/2}$) can be written in terms of the normal and shear displacement discontinuities (Shou and Crouch 1995; Marji 2013; Behnia et al. 2013) obtained for the last special crack tip element as:

$$K_I = \frac{\mu}{4(1-\nu)}\left(\frac{2\pi}{\ell_1}\right)^{\frac{1}{2}}\mathrm{DD}_y(\ell_1), \quad \text{and} \quad K_{II} = \frac{\mu}{4(1-\nu)}\left(\frac{2\pi}{\ell_1}\right)^{\frac{1}{2}}\mathrm{DD}_x(\ell_1) \quad (5)$$

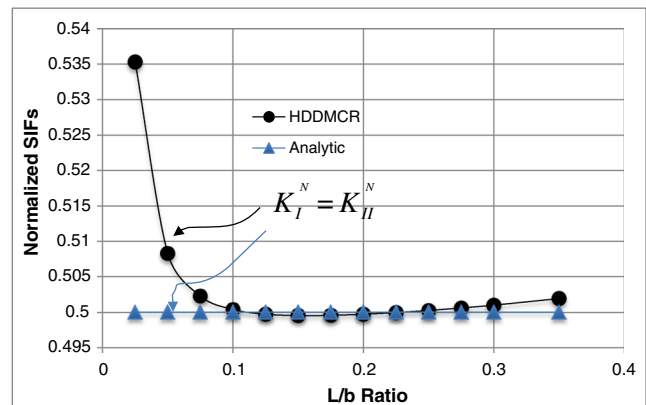where μ is the shear modulus and ν is Poisson's ratio of the brittle material.

Fig. 7 The normalized SIFs, $\left(K_I^N = K_{II}^N\right)$, for the 45° center crack ($\varphi = 45°$), using different L/b ratios

Verification of the modified HDDM

Verification of the modified HDDM is made through the solution of the center slant cracks problems in finite and infinite planes under uniaxial compression. The analytical solution for a center slant crack in an infinite body is given in the rock fracture mechanics literature (Park 2008). Due to simplification of this analytical solution, the validity of the HDDMCR^{2D} code can be obtained by comparing the numerical results with their corresponding analytical results as explained in the following sub-sections.

Center slant crack in an infinite plane

Verifying the center slant crack in an infinite body, a schematic crack with length of $2b$ is considered in a 2D infinite plane as shown in Fig. 4. The crack inclination angle, φ, changes counterclockwise from the x axis, and the compressive stress is acting parallel to the y axis at infinity.

According to the analytical solution (Park 2008), the Mode I and Mode II fracture toughness of an infinite specimen can be estimated from

$$K_{\mathrm{I}} = -\sigma\sqrt{\pi b}\,\varpi_{\mathrm{I}}$$
$$K_{\mathrm{II}} = -\sigma\sqrt{\pi b}\,\varpi_{\mathrm{II}} \qquad (6)$$

where σ is the compressive stress at crack initiation (MPa), b is half of the crack length (mm), and ϖ_{I} and ϖ_{II} are the non-dimensional coefficients (depending on the crack inclination angle, φ) which can be defined as:

$$\varpi_{\mathrm{I}} = \frac{1 + \cos 2\varphi}{2}$$
$$\varpi_{\mathrm{II}} = \frac{\sin 2\varphi}{2} \qquad (7)$$

As it can be seen in Eqs. (6) and (7), the SIFs of crack tips are affected by the crack geometry such as crack length, b, and crack inclination angle, φ.

Variations of ϖ_{I} and ϖ_{II} for the assumed infinite specimen are illustrated in Fig. 5 with changes in the φ angles. As shown in this figure, ϖ_{I} decreases monotonically with increasing φ angle, while ϖ_{II} has a global maximum value at $\varphi = 45°$. Furthermore, Fig. 5 implies that pure Mode I loading is achieved only at $\varphi = 0$ ($\varpi_{\mathrm{I}} = 1$, $\varpi_{\mathrm{II}} = 0$), whereas pure Mode II loading is obtained at $\varphi = 45$ ($\varpi_{\mathrm{I}} = 0.5$, $\varpi_{\mathrm{II}} = 0.5$).

The normalized Mode I and Mode II SIFs are simplified as

$$K_{\mathrm{I}}^{N} = \frac{K_{\mathrm{I}}}{\sigma\sqrt{\pi b}}$$
$$K_{\mathrm{II}}^{N} = \frac{K_{\mathrm{II}}}{\sigma\sqrt{\pi b}} \qquad (8)$$

The mechanical properties of the rock-like specimens (obtained experimentally in a rock mechanics laboratory and

Table 2 The calculated values of the K_{I}^{N} and K_{II}^{N} for different φ angles

φ	K_{I}^{N}		K_{II}^{N}	
	Analytic	HDDMCR^{2D}	Analytic	HDDMCR^{2D}
10	0.9698	0.9699	0.1710	0.1710
20	0.8830	0.8831	0.3213	0.3214
30	0.7500	0.7511	0.4330	0.4320
40	0.5868	0.5861	0.4924	0.4928
50	0.4131	0.4132	0.4924	0.4924
60	0.2500	0.2500	0.4330	0.4330
70	0.1169	0.1170	0.3213	0.3214
80	0.0301	0.0301	0.1710	0.1710

used in all of the analysis conducted in this research) are presented in Table 1. The fracture toughness, K_{IC}, for the tested specimens has been measured in the laboratory by using the well-known formula given in Eq. (5).
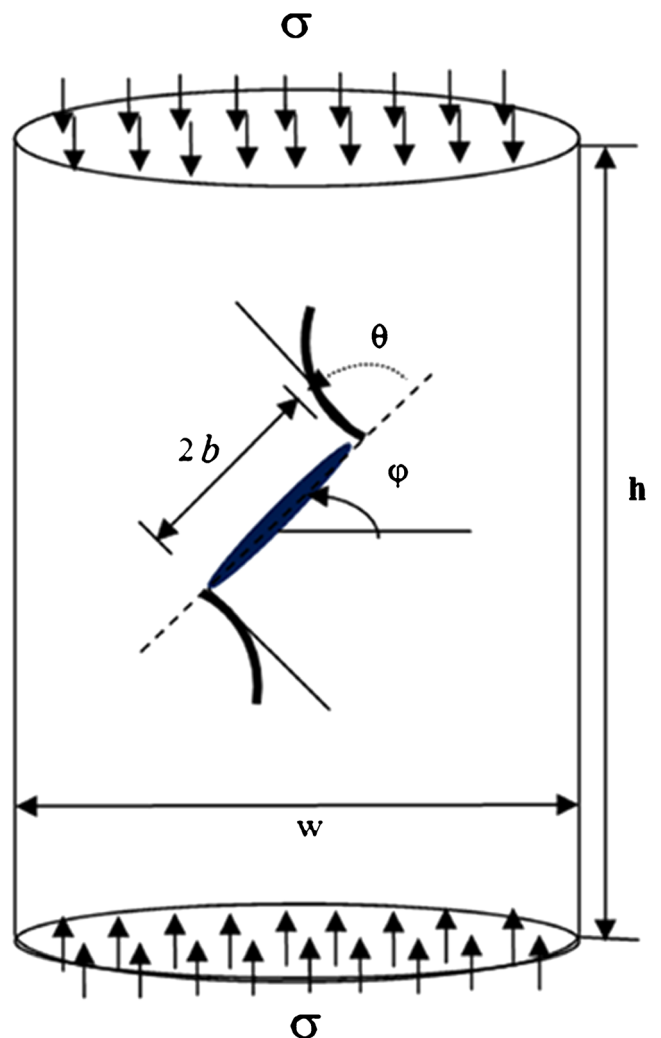

Fig. 8 A center slant crack in a finite plate with ratio $L/w = 2$

Table 3 The numerical values of the K_I^N and K_{II}^N using different b/w ratios ($\varphi = 10°$)

b/w	HDDMCR²ᴰ (finite)		Analytic (infinite)		Difference of finite and infinite planes	
	K_I^N	K_{II}^N	K_I^N	K_{II}^N	K_I^N (finite)–K_I^N (infinite)	K_{II}^N (finite)–K_{II}^N (infinite)
0.01	0.9733	0.1710	0.9698	0.1710	0.0035	0.0000
0.03	0.9744	0.1711	0.9698	0.1710	0.0046	0.0001
0.06	0.9780	0.1716	0.9698	0.1710	0.0082	0.0006
0.09	0.9840	0.1724	0.9698	0.1710	0.0142	0.0014
0.2	1.0264	0.1781	0.9698	0.1710	0.0566	0.0071
0.4	1.1821	0.1975	0.9698	0.1710	0.2123	0.0265
0.6	1.4363	0.2249	0.9698	0.1710	0.4665	0.0539
0.9	2.2251	0.3872	0.9698	0.1710	1.2553	0.2162

The problem shown in Fig. 4 is numerically solved (considering a 45° center slant crack, i.e., $\varphi = 45°$) by the proposed boundary element method (HDDMCR²ᴰ code). The normalized stress intensity factors K_I^N and K_{II}^N are the same for this problem, i.e., $\left(K_I^N = K_{II}^N = 0.5\right)$. Figure 6 compares the numerical and analytical values of the normalized SIFs, $\left(K_I^N = K_{II}^N\right)$, using different number of elements along the crack. The figure illustrates the high accuracy of the proposed boundary element method by using a relatively small number of elements (about 10 quadratic displacement discontinuity elements).

Effect of the ratio of crack tip element length, L, to the half crack length, b (L/b ratio), for $\varphi = 45°$ is shown in Fig. 7. As shown in this figure, the L/b ratios between 0.1 and 0.2 give accurate results, and throughout this text a constant L/b ratio equal to 0.2 has been used.

The numerical and analytical results of K_I^N and K_{II}^N are given in Table 2 considering a center slant crack with different inclinations. This table illustrates the accuracy and usefulness of HDDMCR²ᴰ code for crack analysis.

In the numerical analysis of the present problem, 10 quadratic elements along the pre-existing crack, three special crack tip elements, and $L/b = 0.2$ are used.

Table 2 demonstrates that HDDMCR²ᴰ code gives very accurate results for the center slant crack problem. Thus, the proposed numerical method may be considered as a suitable tool for the analysis of cracks propagation and breakage process in brittle materials.

Center cracks in a finite plane

Consider a rock-like specimen with a center slant crack in a finite plate having a ratio of length, h, to the width, w, equal to 2 (as shown in Fig. 8). Details of the mechanical properties of this finite specimen are the same as those already given in Table 1.

Effect of the specimen boundary on the crack propagation mechanism of a single crack in a finite plate is studied using HDDMCR²ᴰ code by choosing φ angles as 10°, 30°, and 45°. The numerical values of K_I^N and K_{II}^N for different b/w ratios are presented in Tables 3, 4, and 5. The ratios of b to w are taken as: $\frac{b}{w} = 0.01, 0.03, 0.06, 0.09, 0.2, 0.4, 0.6, 0.9$

Table 4 The numerical values of the K_I^N and K_{II}^N using different b/w ratios ($\varphi = 30°$)

b/w	HDDMCR²ᴰ (finite)		Analytic (infinite)		Difference of finite and infinite planes	
	K_I^N	K_{II}^N	K_I^N	K_{II}^N	K_I^N (finite)–K_I^N (infinite)	K_{II}^N (finite)–K_{II}^N (infinite)
0.01	0.7538	0.4322	0.75	0.4330	0.0038	−0.0008
0.03	0.7546	0.4326	0.75	0.4330	0.0046	−0.0004
0.06	0.7573	0.4338	0.75	0.4330	0.0073	0.0008
0.09	0.7617	0.4357	0.75	0.4330	0.0117	0.0027
0.2	0.7930	0.4494	0.75	0.4330	0.0430	0.0164
0.4	0.9137	0.4984	0.75	0.4330	0.1637	0.0654
0.6	1.1297	0.5757	0.75	0.4330	0.3797	0.1427
0.9	1.7236	0.7853	0.75	0.4330	0.9736	0.3523

Table 5 The numerical values of the K_I^N and K_{II}^N using different b/w ratios ($\varphi = 45°$)

b/w	HDDMCR^{2D} (finite)		Analytic (infinite)		Difference of finite and infinite planes	
	K_I^N	K_{II}^N	K_I^N	K_{II}^N	K_I^N (finite)–K_I^N (infinite)	K_{II}^N (finite)–K_{II}^N (infinite)
0.01	0.5043	0.4991	0.5000	0.5000	0.0043	−0.0009
0.03	0.5048	0.4995	0.5000	0.5000	0.0048	−0.0005
0.06	0.5065	0.5008	0.5000	0.5000	0.0065	0.0008
0.09	0.5092	0.5047	0.5000	0.5000	0.0092	0.0047
0.2	0.5428	0.5242	0.5000	0.5000	0.0428	0.0242
0.4	0.6083	0.5719	0.5000	0.5000	0.1083	0.0719
0.6	0.7588	0.6619	0.5000	0.5000	0.2588	0.1619
0.9	1.2296	0.8805	0.5000	0.5000	0.7296	0.3805

According to the results presented in Tables 3, 4, and 5, it can be concluded that with enhancing the b/w ratio more than about 0.2, the normalized SIFs also increase sharply. Alternatively, for the b/w ratios lower than about 0.2, the SIFs tend to their corresponding analytical values for the infinite body case (as it is physically expected). It is found that when the cracks approach to the left and right sides of the specimen, the SIFs increased. It should be noted that the difference between the values of K_I^N and K_{II}^N for the finite and infinite bodies may be negligible for the b/w ratios lower than about 0.2.

Experimental investigation

Preparation of specimen

Initiation, propagation, and coalescence of the pre-existing cracks in rocks have been experimentally investigated by many researchers (Park 2008; Park and Bobet 2009, 2010).

One of the most difficult tasks in experimental investigations is the preparation of specimens containing cracks. In this study, some rock-like specimens are prepared by mixing PPC, fine sand, and water (which are mixed in suitable ratios). The diameter and length of the specimens prepared for experimental tests are 58 and 116 mm, respectively (Fig. 9).

It should be noted that the mechanical properties of the rock-like specimens are obtained from the laboratory tests as presented in Table 1.

Uniaxial compression tests are conducted on rock-like specimens containing two random cracks. The positions of the random cracks may be different in various specimens. These cracks are generated by inserting two thin steel shims with 10 mm width and 1 mm thickness in a mold before casting the specimens. The loading rate was kept at 0.004 mm/min.

A schematic view of the geometry of two random cracks (studied in this research) is depicted in Fig. 10. The crack tips are located on the right and left sides of the crack and indicated by the symbols R and L, respectively. The locations of cracks are also determined by the position of the crack tips.

Fig. 9 A typical rock-like specimen prepared for the laboratory test

Fig. 10 Schematic view of the geometry of two random cracks
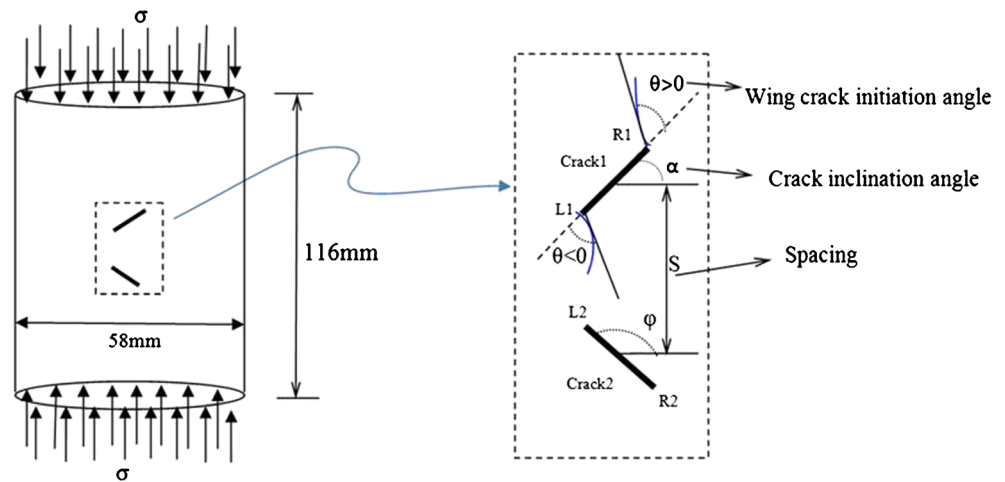
Two random cracks, 1 and 2, with different locations are shown in Fig. 11. The crack geometries are defined by three parameters namely α and φ showing the crack inclination angles of the two cracks (crack 1 and crack 2), respectively, and spacing (S) is the vertical distance between the centers of two cracks expressed in millimeters. The pre-existing random cracks 1 and 2 considered here may have the following parameters (Fig. 11).

Crack inclination angle (α): 40°, 80°, 92°, 110°, 160°, 130°
Crack inclination angle (φ): 24°, 40°, 42°, 110°, 155°, 159°
Spacing (S): 25, 27, 28, 30

Experimental results

Wing and secondary cracks

In this section, the uniaxial compressive tests are carried out on rock-like specimens containing two random cracks. Two types of cracks are observed in these tests: wing cracks and secondary cracks (Fig. 12). Most of the wing cracks observed in these figures are initiated near or at the original tips of the cracks and propagated in a curved path. In addition, these wing cracks are propagated in a stable manner and are approximately propagated parallel to the loading direction. In the experimental tests, the secondary cracks do not always appear, but the wing cracks appeared instantaneously. Secondary cracks are usually initiated after the wing crack propagation and appear at or nearby the tips of the original cracks.

Wing cracks may start their initiation at stress levels of about one half of the specimen's strength. Secondary cracks occurred approximately near the peak strength of the specimens and may extend in an unstable manner. In fact, the stress incremental rate may have a great influence on the propagation of the secondary cracks. In addition to the load incremental rate, the extension of secondary cracks can also depend on the materials types. Figure 12 shows the observed wing cracks

Fig. 11 Crack geometries with different crack inclination angles and spacings
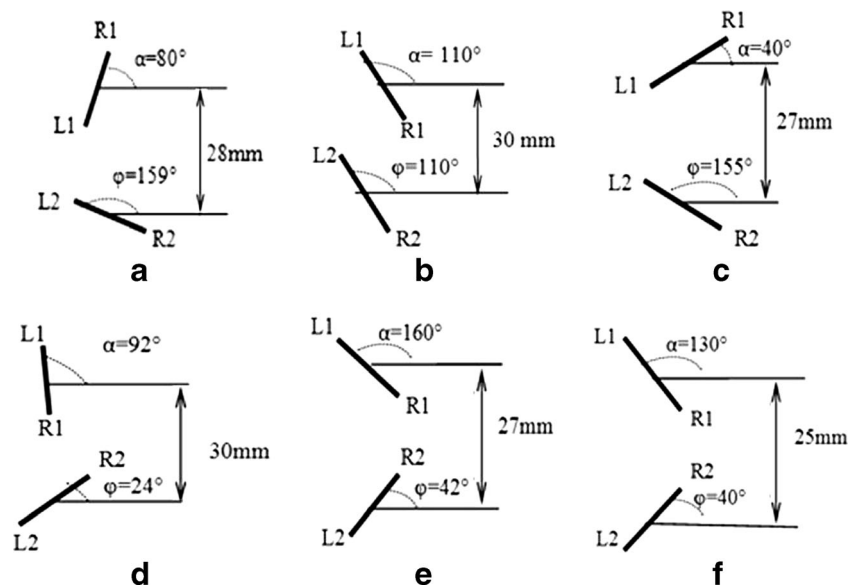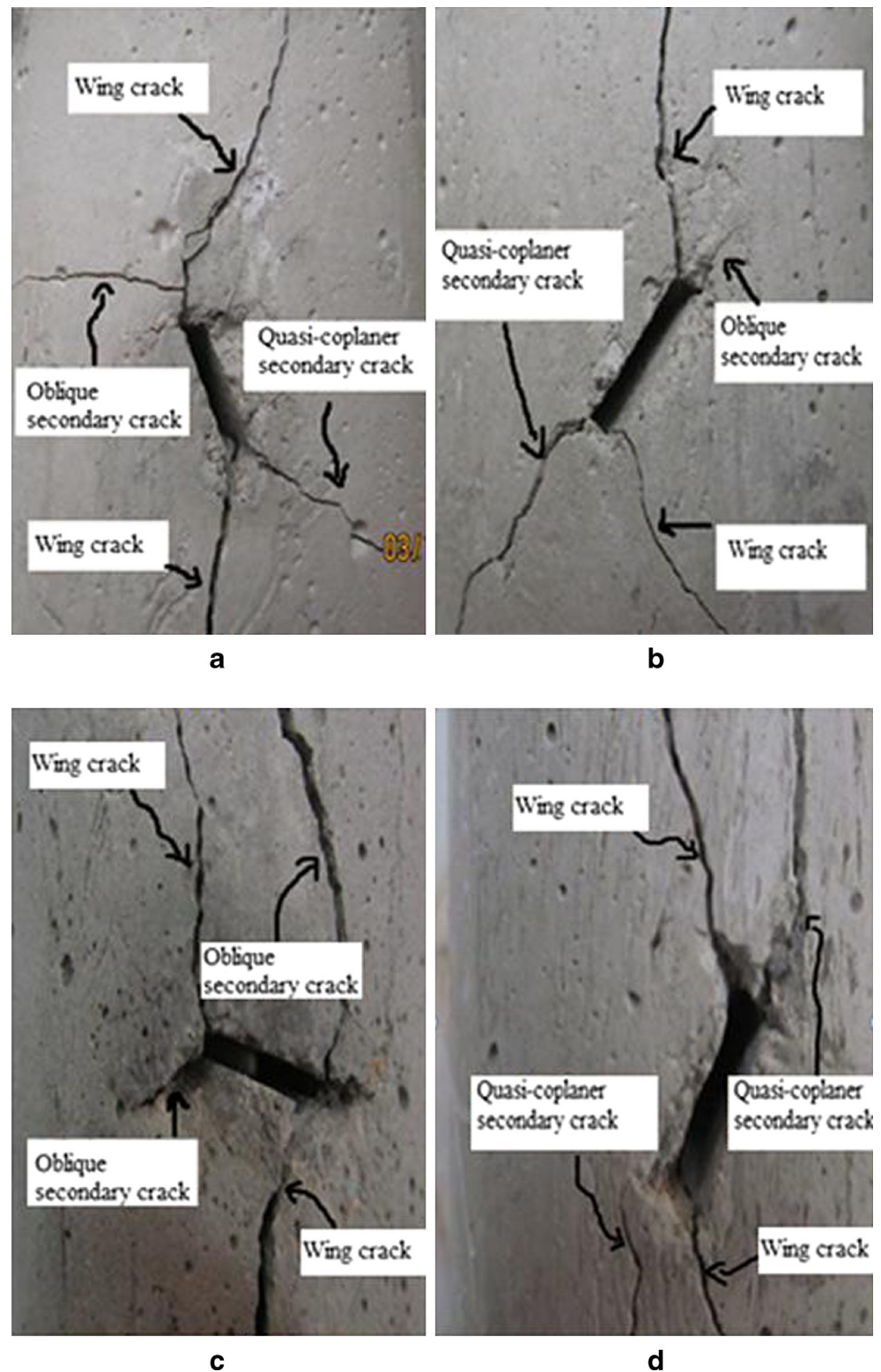
Fig. 12 Specimens showing the propagation of wing crack and two different types of secondary cracks

and the two types of secondary cracks for the specimens containing two random cracks with different inclination angles. In some cases, the two different secondary crack types are observed at the same time. Examples of the quasi-coplanar and oblique secondary cracks are also shown in Fig. 12.

Crack coalescence and breakage process of rock-like specimens

A specific fracture pattern has been occurred in rock-like specimens under uniaxial compression. It means that the wing

and secondary cracks that are initiated and developed from two pre-existing cracks are coalesced leading to the final specimen breakage.

In the current experiments, as the loading condition is quasi-static, the wing cracks are instantaneously initiated (Fig. 13). Therefore, the development and coalescence of wing cracks may be the main cause of the breakage process in rock-like specimens before the secondary cracks can be developed and coalesced with the wing cracks. Figure 13 illustrates six final breakage paths due to the linkage of the wing cracks that are observed in the experiments.

Numerical results

Since the experimental analysis of crack propagation is somewhat time consuming, expensive, difficult, and complex, thus, in this study, the numerical simulation of crack propagation process is also accomplished by HDDMCR^{2D} code.

The same rock-like specimens containing two random cracks (studied experimentally in "Crack coalescence and breakage process of rock-like specimens" section) are also modeled by HDDMCR^{2D} code. The SIFs near the tips of the original cracks and the breakage paths have been estimated
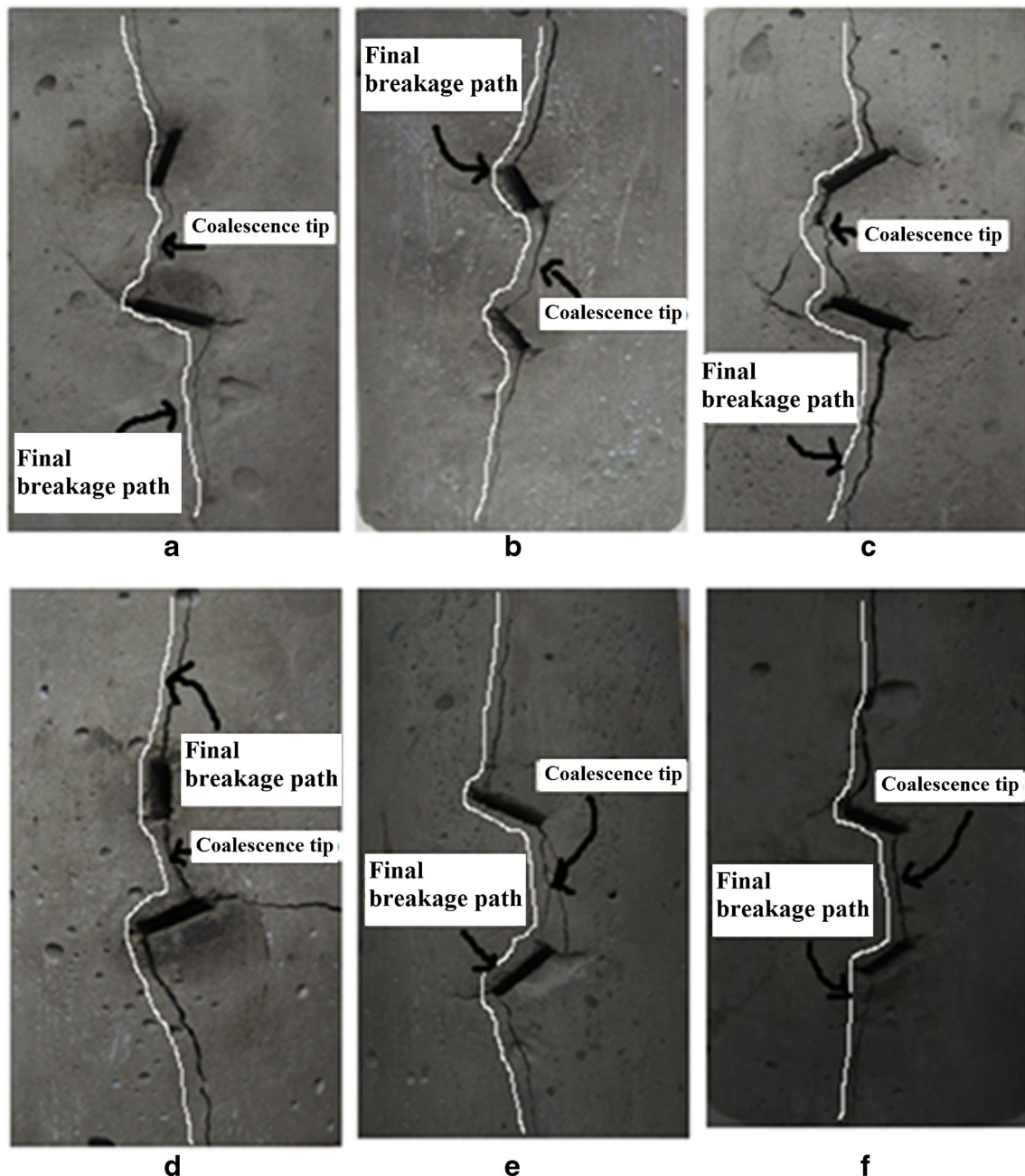

Fig. 13 Experimental modeling results illustrating the final breakage path of rock-like specimens

numerically. The proposed code has also the potential of predicting the wing cracks and specimen breakage due to cracks coalescence.

In the coalescence process of the two random cracks, the crack propagation angle θ for each crack has been calculated in different steps in which the incremental crack length in the direction of θ is extended about 2 mm in each step. In the numerical modeling, the ratio of crack tip length to the crack length equals 0.2 ($L/b = 0.2$). In addition, the discretization of the cracking boundaries have been accomplished by using 10 quadratic elements along each pre-existing crack, two quadratic elements along each crack increment, and a crack tip element is also added to the last crack increment. Figure 14 shows the final breakage paths of the specimens predicted by the numerical simulation.

The experimental observations of the final specimen breakage path (Fig. 13) are used for verifying the numerical simulation of the modeled specimens (Fig. 14). As depicted in these figures (Figs. 13 and 14), there is a good agreement between the experimental and numerical breakage paths predictions for the rock-like specimens.

In the numerical analysis, the values of K_{I}^{N} and K_{II}^{N}, and the wing crack initiation angle (θ) near the original tips of the two random cracks are estimated (in addition to the final breakage paths of rock like-specimens). The values of K_{I}^{N}, K_{II}^{N}, and θ are obtained for the first step of crack propagation process. Table 6 presents the values of K_{I}^{N}, K_{II}^{N}, and θ at each of the four tips of the two cracks.

Interaction between the two random cracks may cause changing in the values of K_{I}^{N} and K_{II}^{N} at different locations
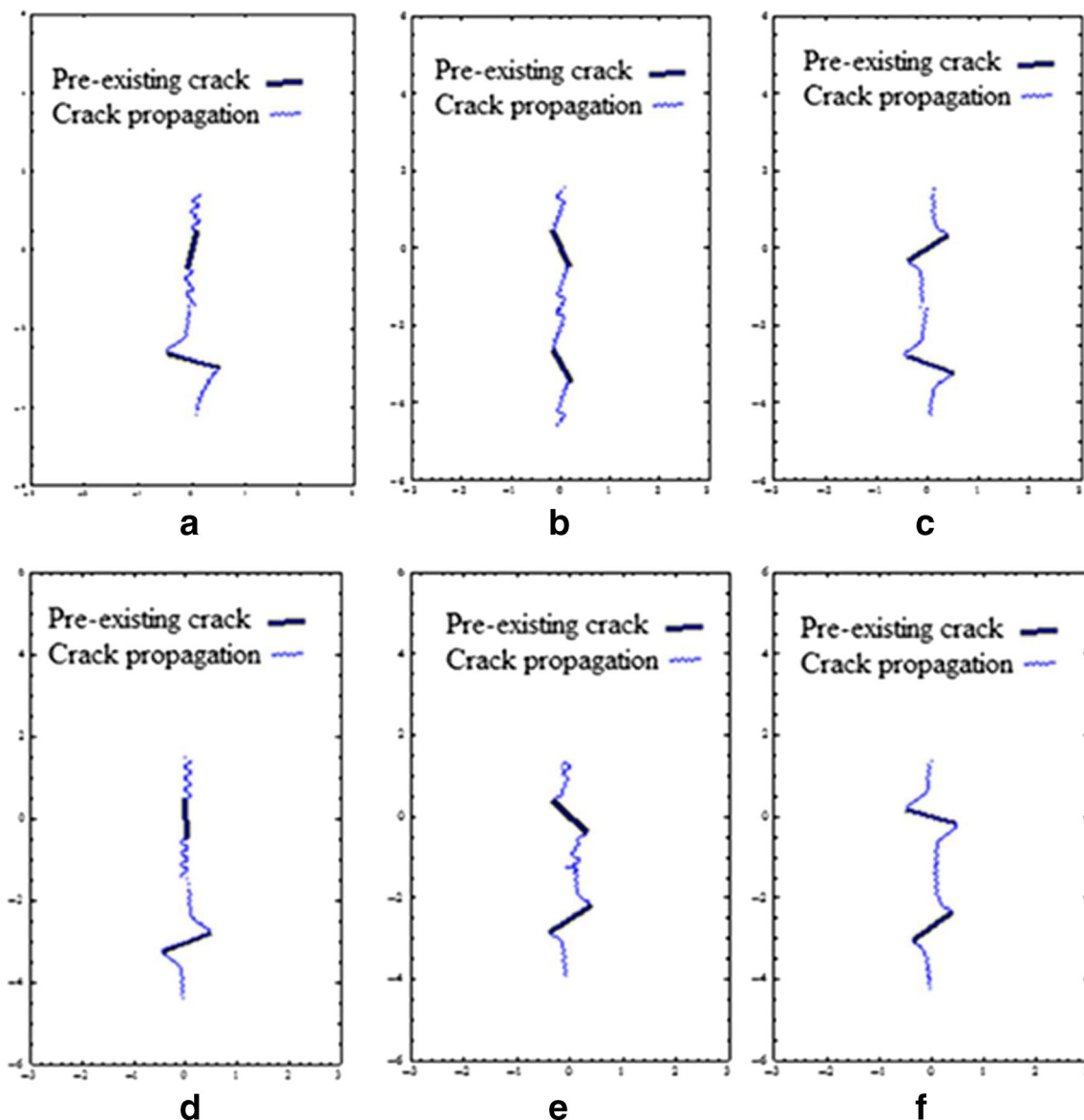

Fig. 14 2D final breakage paths in numerical modeling in different steps

Table 6 Numerical values of K_I^N, K_{II}^N, and θ for four crack tips of two pre-existing cracks

Crack geometry		Spacing (mm)	K_I^N		K_{II}^N		Wing crack initiation angle θ (°)	
			Left	Right	Left	Right	Left	Right
A	$\alpha=80°$	28	0.0398	0.0392	0.1565	0.1631	−75.45	75.17
	$\varphi=159°$		0.8947	0.8498	0.2189	0.3839	132.34	−110.86
B	$\alpha=110°$	30	0.1242	0.1258	0.3284	0.3280	77.87	−77.97
	$\varphi=110°$		0.1289	0.1288	0.3279	0.3281	78.16	−78.15
C	$\alpha=40°$	27	0.5797	0.5876	0.4812	0.4780	−93.86	94.31
	$\varphi=155°$		0.8250	0.8312	0.3887	0.3806	109.48	−110.41
D	$\alpha=92°$	30	0.0115	0.0140	0.0295	0.0267	78.08	−80.76
	$\varphi=24°$		0.8597	0.8583	0.3764	0.3785	−111.90	111.66
E	$\alpha=160°$	27	0.8768	0.8746	0.3180	0.3275	118.37	−117.25
	$\varphi=42°$		0.5581	0.5415	0.4824	0.4818	−92.96	92.34
F	$\alpha=130°$	25	0.4107	0.3982	0.4796	0.4764	87.23	−86.83
	$\varphi=40°$		0.5880	0.5789	0.4872	0.4920	−93.90	93.33

of the cracks (especially at the crack tip). The numerical results demonstrate that the final specimen breakage paths are strongly dependent on the crack location (i.e., for parallel and non-parallel cracks). It is also concluded that for the closer crack tips, the values of K_I^N and K_{II}^N increases.

Table 7 compares the numerical and experimental results considering the cracks initiation and cracks coalescence stresses. The wing crack initiation stresses for various samples changes from 8.3 to 15.8 MPa for the numerical approach and from 7.3 to 14.1 MPa for the experimental works. The cracks coalescence stress changes from 21.8 to 25.3 MPa for the numerical analysis and from 20.3 to 23.2 for the experimental analysis.

Discussions and conclusions

Brittle substances such as rocks may break quasi-statically due to the initiation, propagation, and coalescence of the pre-existing cracks within the body under various loading conditions. In this research, a combined phenomenological framework is presented for rock breakage mechanism in rock-like specimens as the brittle materials. A simultaneous numerical–experimental analysis of crack propagation and cracks coalescence process of rock-like samples have been studied. The Mode I and Mode II stress intensity factors (SIFs) of the pre-existing cracks and propagating wing cracks have been estimated numerically using a numerical code based on the HDDMCR^{2D} analysis. The maximum tangential stress

Table 7 Comparison of wing crack initiation and cracks coalescence stresses (using the HDDMCR^{2D} code and the experiments works)

Crack geometry		Spacing (mm)	Wing crack initiation stress (MPa)		Cracks coalescence stress (MPa)	
			HDDMCR^{2D}	Experiments	HDDMCR^{2D}	Experiments
A	$\alpha=80°$	28	15.8	14.1	25.3	23.2
	$\varphi=159°$		8.3	7.8		
B	$\alpha=110°$	30	15.2	13.4	25	23.1
	$\varphi=110°$		15.2	13.6		
C	$\alpha=40°$	27	11.3	9.8	23.7	21.5
	$\varphi=155°$		9.6	7.3		
D	$\alpha=92°$	30	14.5	12.4	24.4	22.5
	$\varphi=24°$		9.4	8.6		
E	$\alpha=160°$	27	8.6	7.8	23.5	21.8
	$\varphi=42°$		10.4	8.9		
F	$\alpha=130°$	25	12.4	10.6	21.8	20.3
	$\varphi=40°$		10.3	8.5		

criterion is used to estimate the crack propagation angle and its direction of propagation (crack propagation path). The final breakage path of the rock-like specimens with two random cracks has been studied experimentally and it has been demonstrated (in various tables and figures) that these experimental results are in good agreement with the corresponding numerical results estimated by the proposed computer code.

The accuracy of the numerical results is verified by solving some numerical and analytical problems in finite and infinite planes. The corresponding experimental, numerical, and analytical results obtained for some specific problems are compared in several tables and figures showing the validity and reliability of the numerical results.

Six breakage path patterns are observed in the experimental results on rock-like specimens (with two cracks). These patterns are mainly produced through the linkage of two wing cracks (stable breakage path). Breakage patterns of rock-like specimens containing two random cracks are also predicted well by the numerical models through a standard iterative method.

Comparing the parallel and non-parallel cracks, the effect of original crack inclinations of two cracks shows that K_{I}^{N} and K_{II}^{N} (normalized SIFs) have a strong influence on the final specimen breakage path. The normalized SIFs increase with decreasing of the distance between the two crack tips in a specimen. Finally, the numerical results of cracks initiation and cracks coalescence stresses are also compared with the corresponding experimental results for various cases and shown in Table 7.

The numerical and experimental results presented in this study may be very useful for the recognition of propagation and coalescence mechanism of cracks in the rock mass.

The framework can be extended to the fracture mechanism of rock materials under various loading conditions (e.g., triaxial compressive, tensile, and shear loading) and experiments on different rock materials.

Appendix 1

The integrals and their derivatives used for quadratic displacement discontinuity elements (with equal sub-elements) for finite and infinite plane fracture mechanics problems

Starting from the common potential function $F(x,y)$ expressed by Marji et al. (2006) for the solution of stress and displacement fields at the discretized boundaries using the displacement discontinuity function, $DD_j(\delta)$ given in Eq. (1):

$$F(x,y) = \frac{-1}{4\pi\,(1-\nu)} \int_{-\ell}^{\ell} DD_j(\delta)\ln\left[(x-\delta)^2 + y^2\right]^{\frac{1}{2}} d\delta, \quad j = x,y \quad (9)$$

Inserting the common displacement discontinuity function $DD_j(\delta)$ (Eq. 1) in Eq. (9) gives:

$$F(x,y) = \frac{-1}{4\pi\,(1-\nu)}\left\{\left[\int_{-\ell}^{\ell}\Gamma_1(\delta)\ln\left[(x-\delta)^2 + y^2\right]^{\frac{1}{2}}d\delta\right]DD_j^1\right.$$
$$+ \left[\int_{-\ell}^{\ell}\Gamma_2(\delta)\ln\left[(x-\delta)^2 + y^2\right]^{\frac{1}{2}}d\delta\right]DD_j^2$$
$$\left.+ \left[\int_{-\ell}^{\ell}\Gamma_3(\delta)\ln\left[(x-\delta)^2 + y^2\right]^{\frac{1}{2}}d\delta\right]DD_j^3, j = x,y\right\}$$
$$(10)$$

Inserting the shape functions $\Gamma_1(\delta)$, $\Gamma_2(\delta)$, and $\Gamma_3(\delta)$ in Eq. (10) after some manipulations and rearrangements the following three special integrals are deduced:

$$I_1(x,y) = \int_{-\ell}^{\ell}\ln\left[(x-\delta)^2 + y^2\right]^{\frac{1}{2}} \quad (11)$$
$$d\delta = y(\phi_1 - _2) - (x-\ell)\ln(\eta_1) + (x+\ell)\ln(\eta_2) - 2\ell$$

$$I_2(x,y) = \int_{-\ell}^{\ell}\delta\,\ln\left[(x-\delta)^2 + y^2\right]^{\frac{1}{2}} d\delta$$
$$= xy(\phi_1 - \phi_2) + 0.5(y^2 - x^2 + \ell^2)\ln\frac{\eta_1}{\eta_2} - \ell x \quad (12)$$

$$I_3(x,y) = \int_{-\ell}^{\ell}\delta^2\ln\left[(x-\delta)^2 + y^2\right]^{\frac{1}{2}} d\delta = \frac{y}{3}(3x^2 - y^2)(\phi_1 - \phi_2) \quad (13)$$
$$+ \frac{1}{3}(3xy^2 - x^3 + a^3)\ln(\eta_1) - \frac{1}{3}(3xy^2 - x^3 - \ell^3)\ln(\eta_2)$$
$$- \frac{2\ell}{3}\left(x^2 - y^2 + \frac{\ell^2}{3}\right)$$

Where ϕ_1, ϕ_2, η_1, and η_2 can be defined as:

$$\phi_1 = \arctan\left(\frac{y}{x-\ell}\right), \quad \phi_2 = \arctan\left(\frac{y}{x+\ell}\right), \eta_1 = \left[(x-\ell)^2 + y^2\right]^{\frac{1}{2}} \quad (14)$$

$$\text{and} \quad \eta_2 = \left[(x+\ell)^2 + y^2\right]^{\frac{1}{2}}$$

Appendix 2

The integrals and their derivatives used for three special crack tip elements of equal length for finite and infinite plane fracture mechanics problems

Starting from the common special potential function $F_C(x,y)$ expressed by Marji et al. (2006) for the solution of stress and displacement fields at the crack tip using the displacement discontinuity function, $DD_j(\delta)$ given in Eq. (4):

$$F_C(x,y) = \frac{-1}{4\pi(1-\nu)} \int_{-\ell}^{\ell} DD_j(\delta) \ln\left[(x-\delta)^2 + y^2\right]^{\frac{1}{2}} d\delta, \quad j = x, y \quad (15)$$

Inserting the common displacement discontinuity function, $DD_j(\delta)$ (Eq. 3) in Eq. (15) gives:

$$F_C(x,y) = \frac{-1}{4\pi(1-\nu)}\left\{ \left[\int_{-\ell}^{\ell} \Gamma_{C1}(\delta)\ln\left[(x-\delta)^2 + y^2\right]^{\frac{1}{2}} d\delta\right] DD_j^1 + \right.$$

$$\left[\int_{-\ell}^{\ell} \Gamma_{C2}(\delta)\ln\left[(x-\delta)^2 + y^2\right]^{\frac{1}{2}} d\delta\right] DD_j^2$$

$$\left. + \left[\int_{-\ell}^{\ell} \Gamma_{C3}(\delta)\ln\left[(x-\delta)^2 + y^2\right]^{\frac{1}{2}} d\delta\right] DD_j^3, \quad j = x, y \right.$$

$$(16)$$

Inserting the shape functions $\Gamma_{C1}(\delta)$, $\Gamma_{C2}(\delta)$, and $\Gamma_{C3}(\delta)$ in Eq. (16) after some manipulations and rearrangements the following three special integrals are deduced:

$$I_{C1}(x,y) = \int_{-\ell}^{\ell} \delta^{\frac{1}{2}} \ln\left[(x-\delta)^2 + y^2\right]^{\frac{1}{2}} d\delta, \quad (17)$$

$$I_{C2}(x,y) = \int_{-\ell}^{\ell} \delta^{\frac{3}{2}} \ln\left[(x-\delta)^2 + y^2\right]^{\frac{1}{2}} d\delta$$

$$I_{C3}(x,y) = \int_{-\ell}^{\ell} \delta^{\frac{5}{2}} \ln\left[(x-\delta)^2 + y^2\right]^{\frac{1}{2}} d\delta$$

The derivatives of the integrals, I_{C1}, I_{C2}, are given by Marji et al. (2006) and the first two derivatives of I_{C3} (for three special crack tip element case) can be expressed as:

$$I_{C,x}^3 = x\int_0^{2\ell} \frac{\delta^{\frac{5}{2}}}{\left[(x-\delta)^2 + y^2\right]} d\delta - \int_0^{2\ell} \frac{\delta^{\frac{7}{2}}}{\left[(x-\delta)^2 + y^2\right]} \quad (18)$$

$$d\delta = x\Omega_3 - \Omega_4 \quad I_{C,y}^3 = y\int_0^{2\ell} \frac{\delta^{\frac{5}{2}}}{\left[(x-\delta)^2 + y^2\right]} d\delta = y\Omega_3$$

Where

$$\Omega_3 = \int_0^{2\ell} \frac{\delta^{\frac{5}{2}}}{\left[(x-\delta)^2 + y^2\right]} d\delta = \frac{2}{3}(2a)^{\frac{3}{2}} + 2x\Omega_2 - (x^2 + y^2)\Omega_1 \quad (19)$$

where Ω_1, Ω_2, and the derivatives of Ω_1, are defined by Marji et al. (2006) as:

$$\Omega_1 = \int_{-\ell}^{\ell} \frac{\delta^{\frac{1}{2}}}{\left[(x-\delta)^2 + y^2\right]} d\delta =$$

$$\lambda^{-1}\left[\begin{array}{l} 0.5\left(\cos\varphi - \left(\frac{x}{y}\right)\sin\beta\right)\ln\frac{2\ell - 2\sqrt{2\ell}\,\rho\cos\beta + \lambda^2}{2\ell + 2\sqrt{2\ell}\,\rho\cos\beta + \lambda^2} + \left(\sin\beta + \left(\frac{x}{y}\right)\cos\beta\right)\times \\ \arctan\left(\frac{2\sqrt{2\ell}\,\rho\sin\beta}{\lambda^2 - 2\ell}\right) \end{array}\right]$$

$$(20)$$

$$\Omega_2 = \int_{-\ell}^{\ell} \frac{\delta^{\frac{3}{2}}}{\left[(x-\delta)^2 + y^2\right]} d\delta = \lambda\left[\begin{array}{l} 0.5\left(\cos\beta + \left(\frac{x}{y}\right)\sin\beta\right)\ln\frac{2\ell - 2\sqrt{2\ell}\,\lambda\cos\beta + \lambda^2}{2\ell + 2\sqrt{2\ell}\,\lambda\cos\beta + \lambda^2} + \left(\sin\beta + \left(\frac{x}{y}\right)\cos\beta\right)\times \\ \arctan\left(\frac{2\sqrt{2\ell}\,\rho\sin\beta}{\lambda^2 - 2\ell}\right) \end{array}\right] \quad (21)$$

where $\lambda = (x^2 + y^2)^{\frac{1}{4}}$, and $\beta = 0.5\arctan(y/x)$,
and finally

$$\Omega_4 = \int_0^{2\ell} \frac{\delta^{\frac{7}{2}}}{\left[(x-\delta)^2 + y^2\right]} d\delta = \frac{2}{5}(2\ell)^{\frac{5}{2}} + 2x\Omega_3 - (x^2 + y^2)\Omega_2 \quad (22)$$

References

Afifipour M, Moarefvand P (2013) Failure patterns of geomaterials with block-in-matrix texture: experimental and numerical evaluation. Arab J Geosci. doi:10.1007/s12517-013-0907-4

Al Fouzan F, Dafalla MA (2013) Study of cracks and fissures phenomenon in central Saudi Arabia by applying geotechnical techniques. Arab J Geosci. doi:10.1007/s12517-013-0884-7

Aliabadi MH (1998) Fracture of rocks. Computational Mechanics, Southampton

Aliabadi MH, Rooke DP (1991) Numerical fracture mechanics. Computational Mechanics, Southampton

Behnia M, Goshtasbi K, Marji MF, Golshani A (2011) On the crack propagation modeling of hydraulic fracturing by a hybridized displacement discontinuity/boundary collocation method. J Min Environ 2:1–16 (Shahrood University, Shahrood, Iran)

Behnia M, Goshtasbi K, Marji MF, Golshani A (2013) Numerical simulation of crack propagation in layered formations. Arab J Geosci. doi:10.1007/s12517-013-0885-6

Bobet A, Einstein HH (1998a) Fracture coalescence in rock-type materials under uniaxial and biaxial compression. Int J Rock Mech Min Sci 35:863–888. doi:10.1016/S0148-9062(98)00005-9

Bobet A, Einstein HH (1998b) Numerical modeling of fracture coalescence in a model rock material. Int J Fract 92:221–252. doi:10.1023/A:1007460316400

Bordas S, Rabczuk T, Zi G (2008) Three-dimensional crack initiation, propagation, branching and junction in non-linear materials by an extended meshfree method without asymptotic enrichment. Eng Fract Mech 75:943–960.doi:10.1016/j.engfracmech.2007.05.010

Chen JT, Hong HK (1999) Review of dual boundary elements methods with emphasis on hyper singular integrals and divergent series. Appl Mech Rev ASME 52:17–33. doi:10.1115/1.3098922

Crouch SL, Starfield AM (1983) Boundary element methods in solid mechanics. Allen and Unwin, London

Erdogan F, Sih GC (1963) On the crack extension in plates under loading and transverse shear. J Fluids Eng 85:519–527. doi:10.1115/1.3656897

Ghazvinian A, Nejati HR, Sarfarazi V, Hadei MR (2012) Mixed mode crack propagation in low brittle rock-like materials. Arab J Geosci. doi:10.1007/s12517-012-0681-8

Golshani A, Okui Y, Oda M, Takemura T (2005) Micromechanical model for brittle failure of rock and its relation to crack growth observed in triaxial compression tests of granite. Mech Mater 38:287–303. doi:10.1016/j.mechmat.2005.07.003

Guo H, Aziz NI, Schmidt RA (1990) Linear elastic crack tip modeling by displacement discontinuity method. Eng Fract Mech 36:933–943. doi:10.1016/0013-7944(90)90269-M

Guo H, Aziz NI, Schmidt RA (1992) Rock cutting study using linear elastic fracture mechanics. Eng Fract Mech 41:771–778. doi:10.1016/0013-7944(92)90159-C

Haeri H (2011) Numerical modeling of the interaction between micro and macro cracks in the rock fracture mechanism using displacement discontinuity method. Ph.D. thesis, Department of Mining Engineering, Science and Research branch, Islamic Azad University, Tehran, Iran, during work

Haeri H, Ahranjani KA (2012) A fuzzy logic model to predict crack propagation angle under disc cutters of TBM. Int J Acad Res 4:159–169. doi:10.7813/2075-4124.2013

Haeri H, Shahriar K, Marji MF, Moarefvand P (2013) Modeling the propagation mechanism of two random micro cracks in rock samples under uniform tensile loading. Proceedings of the 13th International Conference on Fracture, Beijing, China, June 16–21

Hoek E, Bieniawski ZT (1965) Brittle rock fracture propagation in rock under compression. South African Council for Scientific and Industrial Research Pretoria. Int J Frac Mech 1:137–155. doi:10.1007/BF00186851

Horii H, Nemat-Nasser S (1985) Compression-induced micro crack growth in brittle solids: axial splitting and shear failure. J Geophys Res 90:3105–3125. doi:10.1029/JB090iB04p03105

Huang JF, Chen GL, Zhao YH, Wang R (1990) An experimental study of the strain field development prior to failure of a marble plate under compression. Tectonophysics 175:269–284. doi:10.1016/0040-1951(90)90142-U

Hussian MA, Pu EL, Underwood JH (1974) Strain energy release rate for a crack under combined mode I and mode II. In: Fracture Analysis. ASTM STP 560. American Society for Testing and Materials, pp. 2–28. doi:10.1520/STP33130S

Ichikawa Y, Kawamura K, Uesugi K, Seo YS, Fujii N (2001) Micro-and macro behavior of granitic rock: observations and viscoelastic homogenization analysis. Comput Methods Appl Mech Eng 191:47–72. doi:10.1016/S0045-7825(01)00244-4

Ingraffea AR (1985) Fracture propagation in rock. In: Bazant Z (ed) Mechanics of geomaterials. Wiley, Hoboken, pp. 219–258

Janeiro RP, Einstein HH (2010) Experimental study of the cracking behavior of specimens containing inclusions (under uniaxial compression). Int J Fract 164:83–102. doi:10.1007/s10704-010-9457-x

Ke CC, Chen CS, Tu CH (2008) Determination of fracture toughness of anisotropic rocks by boundary element method. Rock Mech Rock Eng 41:509–538. doi:10.1007/s00603-005-0089-9

Lee H, Jeon S (2011) An experimental and numerical study of fracture coalescence in precracked specimens under uniaxial compression. Int J Solids Struct 48:979–999. doi:10.1016/j.ijsolstr.2010.12.001

Li H, Wong LNY (2012) Influence of flaw inclination angle and loading condition on crack initiation and propagation. Int J Solids Struct 49:2482–2499. doi:10.1016/j.ijsolstr.2012.05.012

Li T, Yang W (2001) Expected coalescing length of displacement loading collinear micro cracks. Theor Appl Fract Mech 36:17–21. doi:10.1016/S0167-8442(01)00052-0

Li YP, Chen LZ, Wang YH (2005) Experimental research on pre-cracked marble under compression. Int J Solids Struct 42:2505–2516. doi:10.1016/j.ijsolstr.2004.09.033

Ma K, Tang CA, Li LC, Ranjih PG, Cai M, Xu NW (2012) 3Dmodeling of stratified and irregularly jointed rock slope and its progressive failure. Arab J Geosci 6:2141–2163. doi:10.1007/s12517-012-0578-6

Manouchehrian A, Marji MF (2012) Numerical analysis of confinement effect on crack propagation mechanism from a flaw in a pre-cracked rock under compression. Acta Mech Sinica 28:1389–1397. doi:10.1007/s10409-012-0145-0

Marji MF (1997) Modeling of cracks in rock fragmentation with a higher order displacement discontinuity method, Ph.D. thesis, Middle East Technical University, Turkey, Ankara

Marji MF (2013) On the Use of power series solution method in the crack analysis of brittle materials by indirect boundary element method. Eng Fract Mech 98:365–382. doi:10.1016/j.engfracmech.2012.11.015

Marji MF, Dehghani I (2010) Kinked crack analysis by a hybridized boundary element/boundary collocation method. Int J Solids Struct 47:922–933. doi:10.1016/j.ijsolstr.2009.12.008

Marji MF, Hosseinin Nasab H, Kohsary AH (2006) On the uses of special crack tip elements in numerical rock fracture mechanics. Int J Solids Struct 43:1669–1692. doi:10.1016/j.ijsolstr.2005.04.042

Oguni K, Wijerathne L, Okinaka T, Hori M (2009) Crack propagation analysis using PDS-FEM and comparison with fracture experiment. Mech Mater 41:1242–1252. doi:10.1016/j.mechmat.2009.07.003

Oliver J, Huespe AE, Sanchez PJ (2006) A comparative study on finite elements for capturing strong discontinuities: E-FEM vs X-FEM. Comput Methods Appl Mech Eng 195:4732–4752. doi:10.1016/j.cma.2005.09.020

Park CH (2008) Coalescence of frictional fractures in rock materials. Ph.D. thesis, Purdue University West Lafayette, Indiana

Park CH, Bobet A (2009) Crack coalescence in specimens with open and closed flaws: a comparison. Int J Rock Mech Min Sci 46:819–829. doi:10.1016/j.ijrmms.2009.02.006

Park CH, Bobet A (2010) Crack initiation, propagation and coalescence from frictional flaws in uniaxial compression. Eng Fract Mech 77:2727–2748. doi:10.1016/j.engfracmech.2010.06.027

Rabczuk T, Bordas S, Zi G (2007) A three-dimensional meshfree method for continuous multiple-crack initiation, propagation and junction in

statics and dynamics. Comput Mech 40:473–495. doi:10.1007/s00466-006-0122-1

Reyes O, Einstein HH (1991) Failure mechanism of fractured rock—a fracture coalescence model. Proceedings of the 7th ISRM Congress, Aachen, Germany, pp. 333–340

Sagong M, Bobet A (2002) Coalescence of multiple flaws in a rock-model material in uniaxial compression. Rock Mech Min Sci 39: 229–241. doi:10.1016/S1365 1609(02)00027-8

Sahouryeh E, Dyskin AV, Germanovich LN (2002) Crack growth under biaxial compression. Eng Fract Mech 69:2187–2198. doi:10.1016/S0013-7944(02)00015-2

Scavia C (1990) Fracture mechanics approach to stability analysis of crack slopes. Eng Fract Mech 35:889–910. doi:10.1029/95JB00040

Shen, B, Stephansson O (1994) Modification of the G-criterion for crack propagation subjected to compression. Eng Fract Mech 47:177–189. doi: 10.1016/0013-7944(94)90219-4

Shen B, Stephansson O, Einstein HH, Ghahreman B (1995) Coalescence of fractures under shear stress in experiments. J Geophys Res Solid Earth 100:5975–5990. doi:10.1029/95JB00040

Shou KJ, Crouch SL (1995) A higher order displacement discontinuity method for analysis of crack problems. Int J Rock Mech Min Sci Geomech Abstr 32:49–55. doi:10.1016/0148-9062(94)00016-V

Sih GC (1974) Strain–energy–density factor applied to mixed mode crack problems. Int J Fract 10:305–321. doi:10.1007/BF00035493

Stan F (2008) Discontinuous Galerkin method for interface crack propagation. Int J Mater Form 1:1127–1130. doi:10.1007/s12289-008-0178-x

Sukumar N, Moran B, Black T, Belytschko T (1997) An element-free Galerkin method for three dimensional fracture mechanics. Comput Mech 20:170–175. doi:10.1007/s004660050235

Verma AK, Singh TN (2010) Modeling of a jointed rock mass under triaxial conditions. Arab J Geosci 3:91–103. doi:10.1007/s12517-009-0063-z

Whittaker BN, Singh RN, Sun Q (1992) Rock fracture mechanics, principals, design and applications, developments in geotechnical engineering. Elsevier, Amsterdam

Wong RHC, Chau KT (1998) Crack coalescence in a rock-like material containing two cracks. Int J Rock Mech Min Sci 35:147–164. doi:10.1016/S0148-9062(97)00303-3

Wong LNY, Einstein HH (2006) Fracturing behavior of prismatic specimens containing single flaws, Golden Rocks, proceedings of 41st U.S. Symposium on Rock Mechanics (USRMS): 50 Years of Rock Mechanics-Landmarks and Future Challenges, Golden, Colorado

Wong RHC, Chau KT, Tang CA, Lin P (2001) Analysis of crack coalescence in rock-like materials containing three flaws—part I: experimental approach. Int J Rock Mech Min Sci 38:909–924. doi:10.1016/S1365-1609(01)00064-8

Wong RHC, Tang CA, Chau KT, Lin P (2002) Splitting failure in brittle rocks containing pre-existing flaws under uniaxial compression. Eng Fract Mech 69:1853–1871. doi:10.1016/S0013-7944(02)00065-6

Yang SQ (2011) Crack coalescence behavior of brittle sandstone samples containing two coplanar fissures in the process of deformation failure. Eng Fract Mech 78:3059–3081. doi:10.1016/j.engfracmech.2011.09.002

Yang Q, Dai YH, Han LJ, Jin ZQ (2009) Experimental study on mechanical behavior of brittle marble samples containing different flaws under uniaxial compression. Eng Fract Mech 76:1833–1845. doi:10.1016/j.engfracmech.2009.04.005